Lung Metabolic Activation as an Early Biomarker of Acute Respiratory Distress Syndrome and Local Gene Expression Heterogeneity

Tyler J. Wellman, Ph.D., Nicolas de Prost, M.D., Ph.D., Mauro Tucci, M.D., Ph.D., Tilo Winkler, Ph.D., Rebecca M. Baron, M.D., Piotr Filipczak, Ph.D., Benjamin Raby, M.D., M.P.H., Jen-hwa Chu, Ph.D., R. Scott Harris, M.D., Guido Musch, M.D., Luiz F. dos Reis Falcao, M.D., Ph.D., Vera Capelozzi, M.D., Ph.D., Jose G. Venegas, Ph.D., Marcos F. Vidal Melo, M.D., Ph.D.

ABSTRACT

Background: Acute respiratory distress syndrome (ARDS) is an inflammatory condition comprising diffuse lung edema and alveolar damage. ARDS frequently results from regional injury mechanisms. However, it is unknown whether detectable inflammation precedes lung edema and opacification and whether topographically differential gene expression consistent with heterogeneous injury occurs in early ARDS. The authors aimed to determine the temporal relationship between pulmonary metabolic activation and density in a large animal model of early ARDS and to assess gene expression in differentially activated regions.

Methods: The authors produced ARDS in sheep with intravenous lipopolysaccharide ($10\,ng \cdot kg^{-1} \cdot h^{-1}$) and mechanical ventilation for 20 h. Using positron emission tomography, the authors assessed regional cellular metabolic activation with 2-deoxy-2-[(18)F]fluoro-D-glucose, perfusion and ventilation with ^{13}NN-saline, and aeration using transmission scans. Species-specific microarray technology was used to assess regional gene expression.

Results: Metabolic activation preceded detectable increases in lung density (as required for clinical diagnosis) and correlated with subsequent histologic injury, suggesting its predictive value for severity of disease progression. Local time courses of metabolic activation varied, with highly perfused and less aerated dependent lung regions activated earlier than nondependent regions. These regions of distinct metabolic trajectories demonstrated differential gene expression for known and potential novel candidates for ARDS pathogenesis.

Conclusions: Heterogeneous lung metabolic activation precedes increases in lung density in the development of ARDS due to endotoxemia and mechanical ventilation. Local differential gene expression occurs in these early stages and reveals molecular pathways relevant to ARDS biology and of potential use as treatment targets. **(ANESTHESIOLOGY 2016; 125:992-1004)**

Downloaded from http://asa2.silverchair.com/anesthesiology/article-pdf/125/5/992/270813/20161100_0-00031.pdf by guest on 09 April 2024

ACUTE respiratory distress syndrome (ARDS) affects approximately 190,600 patients per year in the United States,[1] with mortality up to 45%.[2] Despite this major burden, ARDS diagnosis has seen limited progress since its initial description in 1967[3] and management is still based on supportive care, with no established therapies targeted at the primary disease processes. Accordingly, there is a pressing need for methods of early detection and treatment.

The conceptual model for ARDS portrays an acute, diffuse, inflammatory lung injury with increased pulmonary vascular permeability and lung density.[2] Diffuse alveolar damage is the histopathologic hallmark, and bilateral opacities on lung imaging, reflective of edema and loss of aeration, are required for clinical diagnosis.[2] In contrast to those concepts of a diffuse process, local pathogenic mechanisms underlie the onset of ARDS, particularly in functionally heterogeneous lungs such as those of humans. Mechanical ventilation, frequently used in patients at risk for ARDS, exposes lungs to spatially

What We Already Know about This Topic

- Acute respiratory distress syndrome, defined by hypoxemia and radiographic infiltrates, is often caused by sepsis, but the relationship among infection, gene activation, inflammation, infiltrates, and histology is uncertain.

What This Article Tells Us That Is New

- Sheep exposed to endotoxemia while mechanically ventilated were studied with computed tomography and positron emission tomography followed by lung biopsy. Metabolic activation preceded radiographic infiltration and was colocalized with gene activation and histologic injury. This provides rationale for therapies directed at metabolic or gene products in acute respiratory distress syndrome.

This article is featured in "This Month in Anesthesiology," page 1A. Corresponding article on page 838. Supplemental Digital Content is available for this article. Direct URL citations appear in the printed text and are available in both the HTML and PDF versions of this article. Links to the digital files are provided in the HTML text of this article on the Journal's Web site (www.anesthesiology.org).

Submitted for publication December 5, 2015. Accepted for publication June 27, 2016. From the Departments of Anesthesia, Critical Care and Pain Medicine (T.J.W., M.T., T.W., G.M., L.F.d.R.F., J.G.V., M.F.V.M.) and Medicine (Pulmonary and Critical Care; R.S.H.), Massachusetts General Hospital, Harvard Medical School, Boston, Massachusetts; Medical Intensive Care Unit, Hôpital Henri Mondor, Assistance Publique - Hôpitaux de Paris, Créteil, France (N.d.P.); Department of Medicine (Pulmonary and Critical Care) (R.M.B., P.F.) and Channing Laboratory (B.R., J.-h.C.), Brigham and Women's Hospital, Harvard Medical School, Boston, Massachusetts; and Laboratory of Histomorphometry and Lung Genomics, University of Sao Paulo, Sao Paulo, Brazil (V.C.).

Copyright © 2016, the American Society of Anesthesiologists, Inc. Wolters Kluwer Health, Inc. All Rights Reserved. Anesthesiology 2016; 125:992-1004

Copyright © 2016, the American Society of Anesthesiologists, Inc. Wolters Kluwer Health, Inc. Unauthorized reproduction of this article is prohibited.
<zdoi;10.1097/ALN.0000000000001334>

heterogeneous injury[4] due to high tidal strain,[5] cyclic airway and alveolar recruitment,[6] stress concentration,[7] gas–liquid interfaces,[8] and overdistention.[9] Lung perfusion is also spatially heterogeneous in ARDS patients,[10] potentially influencing local trafficking of inflammatory cells and mediators.[11] Consequently, localized inflammatory processes should be present and detectable during early ARDS, before a diffuse injury pattern is established. However, investigations on the regional basis of molecular and inflammatory processes underlying the early pathogenic period are scant. If inflammation is the fundamental process leading to pulmonary edema, it should precede lung opacities as ARDS develops. Yet, there is no knowledge on the temporal relationship between detectable inflammatory changes and the onset of increased lung density, the current radiographic diagnostic marker for ARDS. Better understanding of these key temporal and topographic processes may contribute to advance diagnostic and prognostic biomarkers and effective therapies.[12]

In studies using exaggerated tidal volumes and driving pressures during short periods (1.5 to 4 h) of mechanical ventilation,[13,14] we suggested that lung metabolism reflective of inflammation measured with positron emission tomography (PET) using the tracer 2-deoxy-2-[(18)F]fluoro-D-glucose (^{18}F-FDG) might be a valuable imaging biomarker of early lung injury. Yet, the significance of such a biomarker for ventilatory settings and time frames comparable to those present in clinical practice is unknown. In the current study, we used a clinically relevant sheep model submitted to endotoxemia and mechanical ventilation during a long period (20 h) using the standard ARDS Network (ARDSNet) ventilation protocol[15] to reprise the "two-hit" injury often seen in patients. This large animal model allowed us to recapitulate the lung functional heterogeneity observed in humans and account for pathophysiologic changes occurring during time frames relevant to human disease.[16–18] We combined multitracer PET and gene expression techniques to study molecular processes during the early development of ARDS. We hypothesized that lung cellular metabolism and gene expression manifest spatial and temporal heterogeneity in response to distinct regional mechanisms of injury and precede density changes detectable with conventional radiography. Our aims were to (1) investigate whether regional changes in pulmonary metabolic activity precede changes in lung density during early ARDS; (2) characterize the temporal trajectories of the components of that metabolic activity contributing to the regional changes and the related regional lung dysfunction; and (3) determine whether regions with distinct metabolic activity exhibit corresponding differences in underlying gene expression.

Materials and Methods

Experimental Protocol

The experimental approach to imaging and tissue analysis is summarized in figure 1. Animal experiments were approved by the Subcommittee on Research Animal Care at the Massachusetts General Hospital (Boston, Massachusetts). Six pathogen-free sheep (22.8 ± 1.7 kg) in the supine position were anesthetized, paralyzed, intubated, and mechanically ventilated. Anesthesia was maintained with a continuous infusion of ketamine and propofol and fentanyl bolus (1 to 2 μg/kg). Paralysis was established with pancuronium (0.1 mg/kg bolus) at induction and repeated every 90 min (0.02 to 0.04 mg/kg). For monitoring and collection of blood samples, we percutaneously cannulated a femoral artery and introduced a pulmonary artery catheter *via* the jugular vein using sterile techniques.

Animals were in the supine position in the PET scanner (Scanditronix PC4096; General Electric, USA), with the caudal end of the field of view just superior to the dome of the diaphragm. Final positioning was determined after a recruitment maneuver with airway pressure at 40 cm H_2O for 30 s to standardize lung history. Sheep were mechanically ventilated for 20 h using the ARDSNet lower positive end-expiratory pressure (PEEP; low stretch) protocol.[15] Initial settings were as follows: volume control mode, tidal volume = 6 ml/kg; PEEP = 5 cm H_2O; inspired oxygen fraction = 0.3 (adjusted to maintain an arterial oxygen saturation greater than or equal to 90% measured by cooximetry [OSM3; Radiometer, Denmark]); inspiratory-to-expiratory ratio = 1:2; and initial respiratory rate = 18 breaths/min and adjusted to maintain the arterial carbon dioxide partial pressure between 32 and 45 mmHg.

After collection of baseline physiologic and imaging data, an infusion of endotoxin (10 ng · kg^{-1} · min^{-1}, *Escherichia coli* O55:B5; List Biologic Laboratories Inc, USA) was started and continued for the whole experiment. In order to ensure cardiovascular stability while maintaining continuity of the extrapulmonary inflammatory stimulus, an algorithm was followed to manage hypotension with lactated Ringer's solution and reduction in endotoxin infusion (Supplemental Digital Content, http://links.lww.com/ALN/B315). No additional recruitment maneuvers were performed. Physiologic data were collected at baseline and at 4-h intervals.

PET Imaging Protocol and Processing

The PET imaging equipment, protocol, and processing methods have been previously presented in detail.[14,19–21] We collected 15 PET transverse slices of 6.5-mm thickness, which provide three-dimensional information over a 9.7-cm-long field of view, estimated to encompass approximately 70% of the total sheep lung volume.[21] Resulting images consisted of an interpolated matrix of 128 × 128 × 15 voxels with a size of 2.0 × 2.0 × 6.5 mm each. Three different types of PET images were acquired.

1.Transmission scans: these were obtained at baseline (0 h) and at 6 and 20 h using a rotating pin source of ^{68}Ge for 10 min. Transmission scans were used to correct for attenuation in emission scans and to calculate the fraction of gas

Copyright © 2016, the American Society of Anesthesiologists, Inc. Wolters Kluwer Health, Inc. Unauthorized reproduction of this article is prohibited.

Downloaded from http://asa2.silverchair.com/anesthesiology/article-pdf/125/5/992/270813/20161100_0-00031.pdf by guest on 09 April 2024

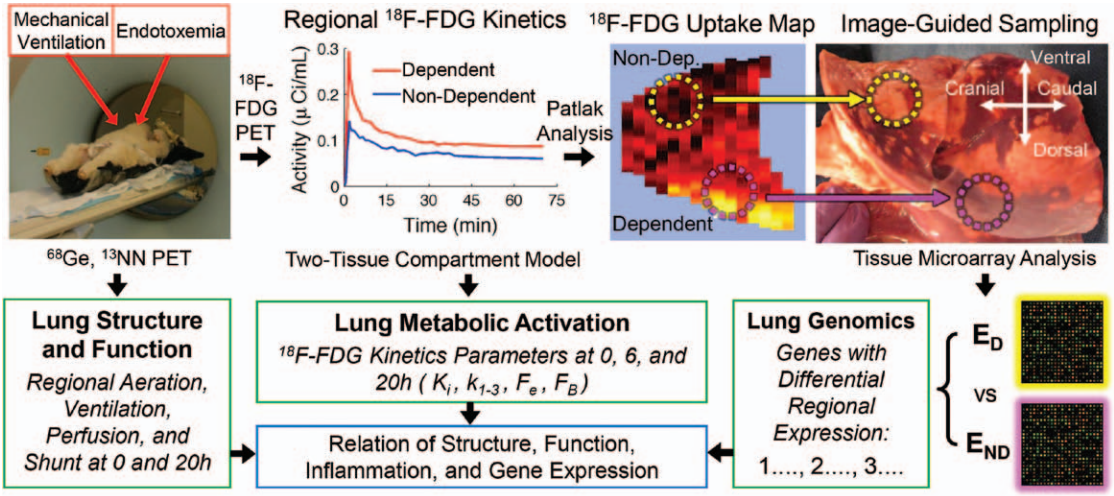

Fig. 1. Schematic overview of the experimental approach. A two-hit model of acute respiratory distress syndrome induced by mechanical ventilation and endotoxemia was studied. Positron emission tomography (PET) was used to assess distributions of regional lung aeration (^{68}Ge), ventilation, and perfusion (^{13}NN). 2-Deoxy-2-[(18)F]fluoro-D-glucose (^{18}F-FDG) kinetics in coregistered regions were analyzed to estimate parameters describing ^{18}F-FDG transport and metabolism and quantify the *in vivo* early inflammatory response. Gene expression levels in regions of distinct metabolic activation were measured to determine genes with differential regional expression. Finally, lung function, inflammation (*i.e.*, metabolic activation), and gene expression were compared to determine potential mechanistic relations between these properties.

(F_{GAS}) of regions of interest (ROIs) from regional tissue density[22] as F_{GAS} = 1 – regional tissue density.

2. ^{13}N-nitrogen emission scans: these were obtained at baseline and at the end of the 20-h mechanical ventilation period for the assessment of regional ventilation, perfusion, and shunt as previously reported with the ^{13}N-nitrogen-saline method.[21,23] The imaging protocol was started with a tracer-free lung. The ventilator was turned off at the end of inhalation, and the airway pressure was equilibrated to a value equal to the mean airway pressure during ventilation. A 30- to 40-ml bolus of ^{13}NN-saline solution was then centrally injected at a rate of 10 ml/s. Simultaneously, collection of a series of consecutive images was started. After an apnea period of 60 s, mechanical ventilation was restarted. The total imaging sequence lasted 4 min and consisted of eight frames of 2.5 s and four frames of 10 s during apnea and six frames of 10 s and four frames of 30 s during the washout phase.

3. ^{18}F-FDG emission scans: after ^{13}NN clearance, ^{18}F-FDG dissolved in 8 ml saline (approximately 40 MBq at 0 h and 200 MBq at 6 and 20 h) was infused at a constant rate through the jugular catheter for 60 s. Starting at the beginning of ^{18}F-FDG infusion, sequential PET frames (9 × 10, 4 × 15, 1 × 30, 7 × 60, 15 × 120, 1 × 300, and 3 × 600 s) were acquired for 75 min. Pulmonary arterial blood was sampled at 5.5, 9.5, 25, 37, and 42.5 min, and plasma activity was measured in a well counter in order to calibrate an image-derived input function for the three-compartment model.[24] Regional ^{18}F-FDG kinetics were fitted to a three-compartment model consisting of an intravascular compartment, a tissue compartment representing the concentration of ^{18}F-FDG available for phosphorylation (*i.e.*, ^{18}F-FDG that is a substrate for hexokinase), and a metabolized compartment accounting for the concentration of ^{18}F-FDG that has been phosphorylated by hexokinase.[25,26] In this analysis, the ^{18}F-FDG net uptake rate (K_i), a measure of cellular metabolic activity, is expressed as $K_i = F_e \cdot k_3$, where k_3 is the rate of ^{18}F-FDG phosphorylation and F_e is the fractional distribution volume of ^{18}F-FDG that is in the tissue but not phosphorylated. In addition, kinetic analysis provides constants k_1 (transfer rate from plasma to tissue), k_2 (transfer rate from tissue to plasma), and F_b (the blood volume fraction in the ROI).

Selection of Voxels for Analysis

Lung masks were created for each animal at three time points (baseline, 6 h, and 20 h) by automatic threshold selection combining aerated regions from transmission scans and perfused regions from ^{13}NN-perfusion scans and subsequent manual refinement to exclude main bronchi and large pulmonary vessels. Masks were divided along the gravitational axis into three adjacent ROIs of equal height (dependent, middle, and nondependent) to quantify regional F_{GAS}, ^{13}NN-saline, and ^{18}F-FDG kinetics.

Transcriptome-wide Gene Expression Analysis

Tissue samples derived from dependent and nondependent regions consistent with high and low ^{18}F-FDG uptake as derived from the PET images were analyzed using microarray analysis.

Total RNA was extracted using the miRNeasy Mini Kit (Qiagen, Germany). RNA quality control assessment was performed using the Agilent 2100 Bioanalyzer (Agilent Technologies, USA). Transcriptome-wide expression was

Copyright © 2016, the American Society of Anesthesiologists, Inc. Wolters Kluwer Health, Inc. Unauthorized reproduction of this article is prohibited.

Downloaded from http://asa2.silverchair.com/anesthesiology/article-pdf/125/5/992/270813/20161100_0-00031.pdf by guest on 09 April 2024

measured with the Agilent Sheep Gene Expression Microarray[27] (Agilent Technologies). This array is customized to assay 15,208 sheep transcripts represented in the NCBI RefSeq (Build 16) and UniGene (Release 27) databases.

For real-time polymerase chain reaction (PCR) validation, total RNA was isolated from frozen lung tissue samples using an RNeasy Mini Kit (Qiagen) according to the manufacturer's standard protocol. During the isolation process, samples were incubated with DNase I (Qiagen) for 15 min at room temperature. The concentration and purity of the isolated RNA were assessed using a NanoDrop 2000 spectrophotometer (Thermo Scientific, USA). TaqMan reverse transcription PCR (RT-PCR) using the QuantiTect Virus Kit (Qiagen) was performed in an ABI Prism 7300 Sequence Real-Time PCR System (Applied Biosystems, USA) using universal thermal cycling parameters. Human-specific TaqMan gene expression assays (Applied Biosystems) were used to measure the messenger RNA levels for plasminogen activator inhibitor-1 (PAI-1), C-X-C motif chemokine ligand 10 (CXCL10), and 18S ribosomal RNA. Each sample was run in duplicate. Gene expression was analyzed using the comparative CT method with 18S ribosomal RNA as the endogenous control.

Histologic Examination and Neutrophil Counts

After euthanasia by exsanguination, the lungs were excised and filled with Trump fixative to 27 cm H_2O. After fixation, tissue blocks from nondependent (ventral) and dependent (dorsal) regions were sampled and analyzed. Samples were collected based on images with differential FDG activity (low nondependent and high dependent).

Light Microscopy. Five-micron hematoxylin–eosin sections were examined by two investigators blinded to the lung region using stereologic point-counting technique[28] at a magnification of ×400 across five random, noncoincident microscopic fields[29] for alveolar, septal and total lung neutrophils, alveolar edema, and hyaline membrane.

Transmission Electron Microscopy. Three 2- × 2- × 2-mm slices cut from nondependent and dependent regions were used to analyze (JEM-1010 transmission electron microscope; JEOL, Japan) the alveolar capillary membrane, neutrophil mitochondria, neutrophil endoplasmic reticulum, and neutrophil lysosomes. Findings were graded with a five-point, semiquantitative, severity-based scoring system as 0 = normal lung parenchyma, 1 = changes in 1 to 25%, 2 = 26 to 50%, 3 = 51 to 75%, and 4 = 76 to 100% of examined tissue.[29]

Statistical Analysis

Data are presented as mean ± SD if normally distributed and median and interquartile interval (25 to 75%) otherwise. Global cardiopulmonary variables were compared using repeated-measures ANOVA with *post hoc* Tukey test for normally distributed data and Kruskal–Wallis test otherwise (SPSS Statistics 21.0 for Mac; IBM Corporation, USA). Imaging measurements were compared with ANOVA using time, region, and time × region as main factors. Tukey honest significant difference test was used for *post hoc* analysis controlling for multiple comparisons (Matlab version R2015b; Mathworks, USA). All statistical tests were two tailed, and significance was set at $P < 0.05$.

Results

Twenty Hours of Protective Mechanical Ventilation and Endotoxemia Produce Global Cardiopulmonary Dysfunction and Inflammation Consistent with ARDS

Respiratory system compliance worsened during 20 h, and oxygenation reached the range of moderate ARDS at 6 h (fig. 2 and table 1), despite increases in PEEP and inspired oxygen fraction according to the ARDSNet protocol. Total fluid administered was 5.0 (4.6 to 5.4) ml · kg^{-1} · h^{-1}. Circulating neutrophils and monocytes decreased by 6 h and recovered by 20 h (fig. 2; table S1, Supplemental Digital Content, http://links.lww.com/ALN/B315).

Optical microscopy revealed infiltration of alveolar and septal neutrophils, alveolar edema, and hyaline membranes (fig. 2; fig. S1 and table S2, Supplemental Digital Content, http://links.lww.com/ALN/B315). Electron microscopy showed mild defects of the alveolar capillary membrane, increased neutrophil lysosomes, and changes in neutrophil mitochondria and endoplasmic reticulum consistent with neutrophil activation (fig. 2; fig. S2 and table S2, Supplemental Digital Content, http://links.lww.com/ALN/B315).

Lung Aeration Is Reduced and Regional Perfusion and Ventilation–Perfusion Ratios Are More Heterogeneous after 20 h of Protective Mechanical Ventilation and Endotoxemia

Whole-lung gas fraction was unaffected from baseline (0.64 ± 0.03) to 6 h (0.66 ± 0.04) and decreased by 6% from 6 to 20 h (0.62 ± 0.05; $P < 0.05$). Regional gas fractions were also unchanged from baseline to 6 h (fig. 3, A and B). F_{GAS} decreased in dependent regions only from 6 to 20 h ($P < 0.05$), despite a significant simultaneous increase in PEEP (fig. 3, A and B, and table 1). Throughout, dependent regions showed lower F_{GAS} (fig. 3B) and higher specific ventilation (= ventilation/volume; fig. 3, C and D) than nondependent regions. Differences in aeration distributions at the voxel level corroborated the regional heterogeneity in lung inflation (fig. S3, Supplemental Digital Content, http://links.lww.com/ALN/B315). These inhomogeneities in local aeration and ventilation imply underlying regional inhomogeneities in the lung mechanical microenvironment.

Regional perfusion was heterogeneously distributed (fig. 3, E and F), even after correcting for tissue density (fig. 3G), highest in dependent regions (fig. 3, F and G). This heterogeneity increased with time (interaction effect for tissue normalized perfusion: ROI × time; $P = 0.017$). Regional differences in perfusion accounted for significant ventilation–perfusion mismatch, as mean ventilation/

Downloaded from http://asa2.silverchair.com/anesthesiology/article-pdf/125/5/992/270813/20161100_0-00031.pdf by guest on 09 April 2024

Copyright © 2016, the American Society of Anesthesiologists, Inc. Wolters Kluwer Health, Inc. Unauthorized reproduction of this article is prohibited.

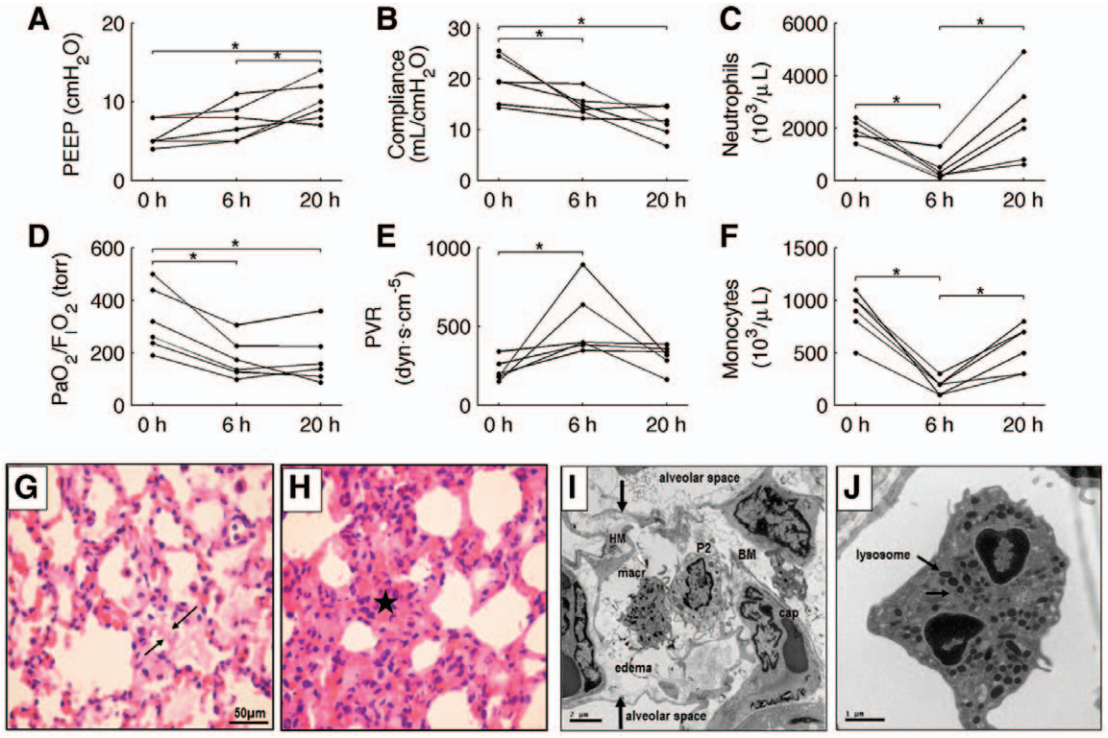

Fig. 2. Twenty hours of mechanical ventilation with the acute respiratory distress syndrome network (ARDSNet) protocol and endotoxin infusion produce deterioration of lung function and gas exchange consistent with ARDS development. Positive end-expiratory pressure (PEEP) levels (*A*), respiratory system compliance (*B*), peripheral blood neutrophil counts (*C*), ratios of arterial oxygen pressure to inspired oxygen fraction (Pao_2/Fio_2) (*D*), pulmonary vascular resistance (PVR) (*E*), and blood monocyte counts (*F*) during 20 h of mechanical ventilation and endotoxin infusion (*$P < 0.05$ between time points). Cardiac output decreased at 6 h and then recovered in parallel with a significant increase in PVR for similar pulmonary capillary wedge pressures, consistent with a vascular response to endotoxemia. Light microscopy showed hyaline membrane formation (*G*), as well as alveolar and septal neutrophils (*H*), consistent with acute inflammation. Transmission electron microscopy revealed edema of the alveolar capillary membrane (*I*), and neutrophils showed increased activity and prominence of lysosomes (*arrows*; *J*).

perfusion was lowest and shunt was highest in dependent regions at baseline and 20 h (fig. 3, H to J).

Regional and Global Increases in Pulmonary Metabolic Activity Precede Rises in Lung Density and Correlate with Histologic Injury

^{18}F-FDG kinetics revealed whole-lung increases in pulmonary metabolic activity (net ^{18}F-FDG uptake, K_i) already at 6 h of endotoxemia and mechanical ventilation, suggestive of early neutrophilic activation. This preceded the increase in whole-lung density, the usual radiographic marker of ARDS, observed at 20 h (fig. 4, A and B). The rise in whole-lung ^{18}F-FDG phosphorylation rate (k_3, fig. 4C) was a major factor underlying the increased net uptake.

Distinct temporal patterns of lung metabolism were present at the regional level (fig. 5, A and B). At baseline, the initially healthy lungs showed homogenous metabolism, with no regional differences in k_3 (fig. 5C; fig. S4 to S6, Supplemental Digital Content, http://links.lww.com/ALN/B315) or K_i normalized by tissue density (K_{iT}, Supplemental Digital Content, http://links.lww.com/ALN/B315). From 0 to 6 h, K_i increased substantially throughout the lungs, particularly in dependent regions (fig. 5, A and B), preceding any detectable lung density changes (fig. 5, A and B; fig. S4, Supplemental Digital Content, http://links.lww.com/ALN/B315). In contrast, during the 6- to 20-h period, nondependent and middle regions were the primary sites of increased metabolic activity, as evidenced by higher K_i and k_3 (fig. 5, B and C). Of note, those early increases in regional k_3 (0 to 6 h) were associated with later increases in lung density (6 to 20 h; fig. 4D).

Examination of K_{iT} indicated that regional tissue density accounted for a minimal portion of the regional temporal changes in ^{18}F-FDG uptake (fig. S5, Supplemental Digital Content, http://links.lww.com/ALN/B315) but significantly influenced the topographic distribution in ^{18}F-FDG uptake (figs. S5 and S6, Supplemental Digital Content, http://links.lww.com/ALN/B315). Thus, by 20 h, tissue-specific measures of metabolic activity (*i.e.*, K_{iT} and k_3) were homogeneously increased in all regions relative to baseline. However, *dependent, middle, and nondependent regions reached an elevated state of metabolism through distinct temporal trajectories*. The association of these metabolic changes with lung aeration indicated differences in the time scale of

Copyright © 2016, the American Society of Anesthesiologists, Inc. Wolters Kluwer Health, Inc. Unauthorized reproduction of this article is prohibited.

Downloaded from http://asa2.silverchair.com/anesthesiology/article-pdf/125/5/992/270813/20161100_0-00031.pdf by guest on 09 April 2024

Table 1. Respiratory and Cardiovascular Variables at Baseline and after 6 and 20 h of Mechanical Ventilation and Endotoxemia

	Baseline	6 h	20 h	*P* Value
Respiratory variables				
F_{IO_2}, %	40 (40–43)	40 (40–53)	60 (40–80)†	0.04
V_T, ml/kg	6.5 (6.3–7.1)	6.4 (6.2–6.9)	6.5 (6.1–7.0)	0.70
PEEP, cm H_2O	5 (5–8)	7 (5–10)	10 (8–13)*†	0.01
RR, min^{-1}	33 (28–36)	35 (33–36)	31 (30–36)	0.59
P_{Peak}, cm H_2O^{-1}	17 ± 3	21 ± 4*	28 ± 6*†	0.01
P_{Plat}, cm H_2O^{-1}	14 ± 3	18 ± 2*	24 ± 5*†	0.01
C_{rs}, ml/cm H_2O	19.7 ± 4.6	14.9 ± 2.3*	11.4 ± 3.0*	0.01
pH_a	7.41 ± 0.06	7.32 ± 0.09*	7.28 ± 0.08*	0.01
$Paco_2$, torr	46 ± 2	47 ± 13	44 ± 7	0.82
Pao_2, torr	133 ± 45	76 ± 26*	95 ± 29	0.01
Pao_2/F_{IO_2}	324 ± 122	177 ± 77*	180 ± 100*	0.01
Pvo_2, torr	49 (45–53)	48 (34–67)	48 (46–57)	0.96
Bicarbonate, mM	29 ± 4	24 ± 6	20 ± 4*	0.01
$ETco_2$, mmHg	43 ± 3	39 ± 5	33 ± 4*†	0.01
Cardiovascular variables				
HR, beats/min	166 ± 35	127 ± 27*	155 ± 22†	0.02
MAP, mmHg	96 (89–98)	78 (75–102)	76 (65–89)*	0.03
MPAP, mmHg	17 ± 4	21 ± 4	20 ± 4	0.17
PCWP, mmHg	4 ± 3	5 ± 2	4 ± 3	0.19
PVR, dynes · s · cm^{-5}	191 (173–281)	400 (374–704)*	329 (255–366)	0.02
CO, L/min	5.0 ± 1.1	2.8 ± 1.1*	4.3 ± 1.4	0.03
SV, ml	30 (26–33)	24 (14–28)	25 (21–35)	0.15
Lactate, n = 4, mM	1.8 (0.8–3.1)	1.0 (0.8–1.9)	1.2 (0.7–1.8)	0.63
Temperature, °F	100.8 ± 0.8	100.3 ± 1.7	98.6 ± 1.6*	0.01

Variables are expressed as mean ± SD for normally distributed variables and median and interquartile range (25 to 75%) otherwise.

*$P \le 0.05$ (*vs.* baseline). †$P \le 0.05$ (*vs.* 6 h).

CO = cardiac output; C_{rs} = compliance of the respiratory system; $ETCO_2$ = end-tidal carbon dioxide; F_{IO_2} = inspired fraction of oxygen; HR = heart rate; MAP = mean arterial pressure; MPAP = mean pulmonary arterial pressure; $PaCO_2$ = arterial partial pressure of carbon dioxide; Pao_2/F_{IO_2} = ratio between arterial partial pressure of oxygen and F_{IO_2}; PCWP = pulmonary capillary wedge pressure; PEEP = positive end-expiratory pressure; P_{Peak} = peak inspiratory pressure; P_{Plat} = plateau airway pressure; Pvo_2 = mixed venous partial pressure of oxygen; PVR = pulmonary vascular resistance; RR = respiratory rate; SV = stroke volume; V_T = tidal volume.

injury development in regions of low aeration versus regions of high aeration (fig. 6).

Quantification of the determinants of ^{18}F-FDG uptake ($K_i = F_e \cdot k_3$) indicated that its rise at 6 and 20 h was due to a larger contribution of increased phosphorylation rate (k_3; fig. 5C) combined with a rise in the ^{18}F-FDG volume of distribution F_e (fig. 5D). Measures of histologic injury at 20 h (lung injury score, septal congestion, and neutrophil counts) were correlated with k_3 at 6 h, suggesting a value for early phosphorylation to signalize ensuing injury (fig. S7, Supplemental Digital Content, http://links.lww.com/ALN/B315).

Gene Expression Patterns Are Regionally Heterogeneous in Early ARDS

We found regional differential expression of 24 distinct annotated genes of the approximately 15,000 specific RNA sequences represented in the microarrays (dependent *vs.* nondependent; $P < 0.001$; fig. 7, A and B). Most of these (75%) showed higher expression in dependent regions. Four genes were previously associated with sepsis (CXCL10 in neonatal sepsis,[30] chitinase 3-like 1 [CHI3L1],[31] complement 3 [C3],[32] and integrin, αL [ITGAL][33]), potentially consistent with higher dependent lung perfusion and endotoxemia in the studied model. In contrast, three genes with higher nondependent expression have been previously related to experimental ventilator-induced lung injury (VILI; PAI-1,[34] amphiregulin,[35] and THBS1[36]), suggesting regional activation of mechanotransduction processes. The gene for CXCL10 demonstrated the most significant differential regional expression (six separate sequences in the used microarray, systematically higher expression in dependent regions; $P < 0.001$). The presence of hyperinflation in nondependent regions (fig. S3, Supplemental Digital Content, http://links.lww.com/ALN/B315) suggests a role for tissue overdistention in eliciting such cellular responses. In fact, expression levels of several VILI-associated genes were correlated with regional hyperinflation (fig. S8, Supplemental Digital Content, http://links.lww.com/ALN/B315). Such findings support the concept of topographically distinct injury mechanisms during early ARDS. Analysis of differentially expressed genes ($P < 0.01$; 174 distinct annotated genes) into gene ontology terms resulted in processes related to regulation of leukocyte activation, regulation of cytokine production, regulation of apoptosis, and immune response (DAVID software,[37] National Institute of Allergy and Infectious Diseases, USA; table S3, Supplemental Digital Content, http://links.lww.com/ALN/B315).

Copyright © 2016, the American Society of Anesthesiologists, Inc. Wolters Kluwer Health, Inc. Unauthorized reproduction of this article is prohibited.

Downloaded from http://asa2.silverchair.com/anesthesiology/article-pdf/125/5/992/270813/20161100_0-00031.pdf by guest on 09 April 2024

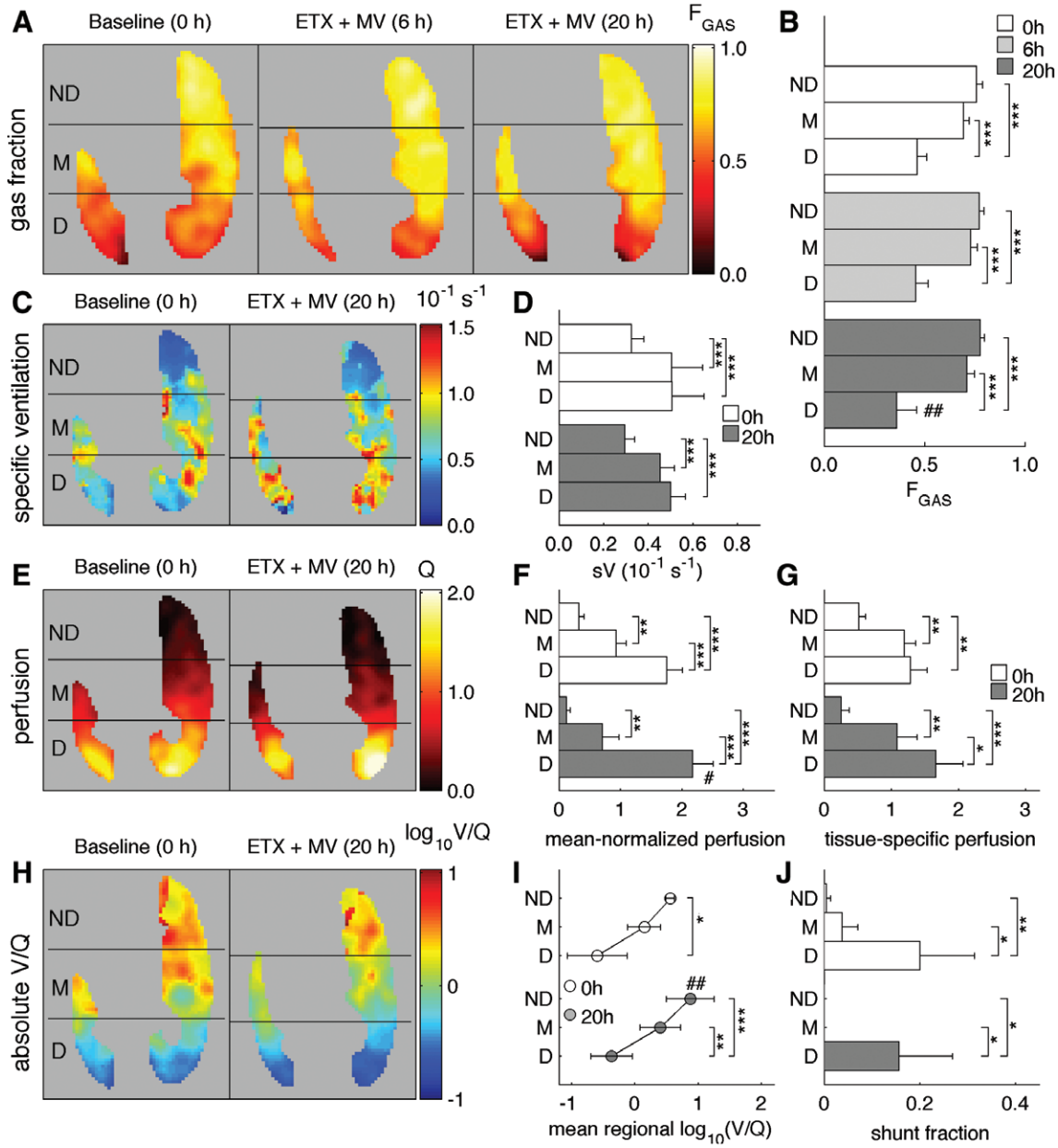

Fig. 3. Spatial heterogeneity in lung function after 20 h of mechanical ventilation (MV) and endotoxemia (ETX) in sheep reflects heterogeneous regional dysfunction typical of acute respiratory distress syndrome patients. Heterogeneous aeration (F_{GAS}) was observed at all time points (*A*), with lower aeration in dependent (D) regions than in middle (M) or nondependent (ND) regions (*B*). Distributions of F_{GAS} and consequently of lung density were stable over time, with only dependent F_{GAS} decreasing from 6 to 20 h. Specific ventilation (sV) was also heterogeneous (*C*), with higher values in M and D regions (*D*). Regional perfusion showed a similar gravitational gradient to sV (*E*), which became more pronounced over time (*F*), even when normalized for tissue (*G*). At both time points, V/Q ratios were significantly lower in dependent regions (*H*, *I*), where the majority of shunt was localized (*J*). $^{*}P < 0.05$, $^{**}P < 0.01$, and $^{***}P < 0.001$ for regional differences. #$P < 0.05$ and ##$P < 0.01$ for differences between time points for the same region.

Microarray results for a gene with higher differential expression in nondependent regions (PAI-1) and another in dependent regions (CXCL10) were validated using the technique of semiquantitative RT-PCR in samples from three sheep (fig. S9, Supplemental Digital Content, http://links.lww.com/ALN/B315). There was clear agreement in the directions of gene expression ratios with median expression for PAI-1 $\log_2(E_{ND}/E_D) = 2.07$ ($P = 0.048$) and for CXCL10 $\log_2(E_{ND}/E_D) = -3.64$ ($P = 0.049$). Throughout, the use of metabolic imaging to guide tissue sampling improved the sensitivity of the analysis by allowing for paired gene expression comparisons in regions of distinct metabolic temporal trajectories, even when interanimal gene expression variability was large

Copyright © 2016, the American Society of Anesthesiologists, Inc. Wolters Kluwer Health, Inc. Unauthorized reproduction of this article is prohibited.

Downloaded from http://asa2.silverchair.com/anesthesiology/article-pdf/125/5/992/270813/20161100_0-00031.pdf by guest on 09 April 2024

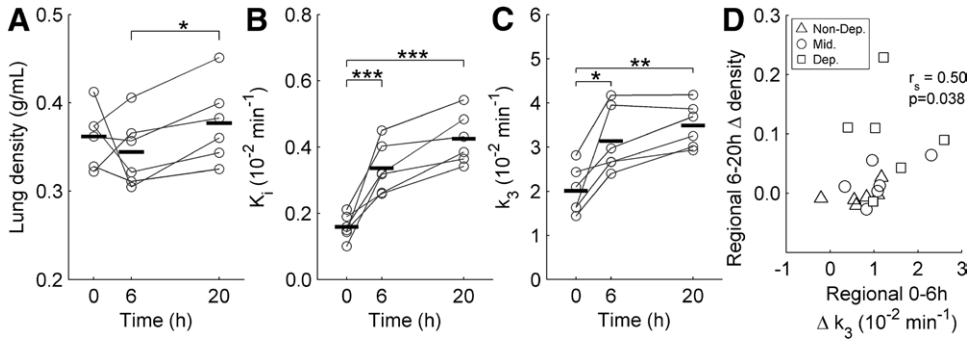

Fig. 4. Whole-lung metabolic activation precedes increases in lung density during early experimental acute respiratory distress syndrome (ARDS). (*A*) Lung density, an important diagnostic measure of ARDS, presented a discrete increase from 6 to 20 h of endotoxemia and mechanical ventilation. (*B*) In contrast, a notable rise in the whole-lung 2-deoxy-2-[(18)F]fluoro-D-glucose (^{18}F-FDG) net uptake rate (K_i) was already evident at 6 h of injury and continued to increase through 20 h. (*C*) The increased ^{18}F-FDG phosphorylation rate (k_3) was an important determinant of that rise in K_i. (*D*) Early regional changes in k_3 correlated with subsequent changes in regional lung density. **P* < 0.05, ***P* < 0.01, and ****P* < 0.001.

(fig. S10, Supplemental Digital Content, http://links.lww.com/ALN/B315).

Discussion

We demonstrate increased *in vivo* whole-lung and regional metabolic activation within the first 20 h of lung injury produced by endotoxemia and mechanical ventilation, which preceded lung density increases routinely utilized for ARDS diagnosis. In lungs of sizes comparable to those of humans, temporal trajectories of metabolic activation were spatially heterogeneous and coregistered with topographic heterogeneity in gene expression. Gene expression patterns not only revealed heterogeneous local activation of injury mechanisms previously reported in more homogeneous rodent models but also identified novel mechanisms and treatment targets potentially relevant to human disease.

Molecular imaging with ^{18}F-FDG PET quantifies glucose uptake, membrane transport, and metabolism by hexokinase. While increased cellular metabolism (^{18}F-FDG uptake) has been observed in established ARDS in patients[38] and animals,[39] little is known for conditions mimicking clinical settings in the early stages of lung injury. Our results revealed a marked and heterogeneous increase in lung metabolic activation as early as 6 h from the onset of endotoxemia and mechanical ventilation. This contrasted with the lack of changes in global or regional lung aeration by 6 h and a small loss of aeration by 20 h. Given that bilateral lung opacities are required for ARDS diagnosis,[2] our results suggest that ^{18}F-FDG kinetics parameters could provide an earlier molecular marker of lung injury than conventional imaging.

The early regional increase in ^{18}F-FDG uptake was due to a rise in both the ^{18}F-FDG phosphorylation rate (k_3) and volume of distribution (F_e) in dependent regions. k_3 has been shown to reflect hexokinase activity in tissues,[40] whereas F_e depends on tissue density, neutrophil numbers, and edema.[26] The contributions of k_3 and F_e to K_i showed substantial regional variation, with a larger k_3 contribution in nondependent regions and a balanced k_3 and F_e contribution in dependent regions. The early (6 h) reduction in circulating neutrophils that accompanied the increase in ^{18}F-FDG uptake suggests that those regional metabolic changes reflected increased neutrophil recruitment and activation. These results are consistent with our observed gene ontology and findings of regulation of phosphorylation and glucose transport and neutrophil chemotaxis in a rat model of lipopolysaccharide-induced lung injury.[34] A smaller metabolic contribution from macrophages, pneumocytes II, and endothelial cells can occur.[41] Overall, our findings imply that by the time ARDS is detected with conventional imaging (as required for diagnosis), the underlying inflammatory response may be already fully developed. Therefore, assessment of regional metabolism in the early stages of lung injury with ^{18}F-FDG PET may be useful to predict disease progression and assess treatment efficacy.

Inflammatory and functional changes from 6 to 20 h differed from those in the first 6 h. Indeed, the increase in k_3 in nondependent regions from 6 to 20 h, indicative of inflammation (fig. 5C), would have been entirely missed if shorter periods had been studied. Accordingly, results from short-term experimental studies, frequently associated with exaggerated nonclinical ventilatory settings,[35,42] may be limited in characterizing the development of ARDS over time scales more representative of its clinical progression.

Importantly, structural and functional heterogeneities present in our model, and typical of ARDS patients, raise the possibility that the observed distinct local time courses of metabolism resulted from topographically heterogeneous injury mechanisms. Glycocalyx degradation in regions of increased blood flow and exposure to endotoxin could facilitate early local neutrophil trafficking, surfactant dysfunction, and lung derecruitment.[43] Such mechanism could compose with cyclic airway and alveolar recruitment,[6] stress concentration,[7] gas–liquid interfaces,[8] high tidal strain,[5] and increased flow of inflammatory cells due to higher dependent lung perfusion in dependent lung regions to produce regional inflammation and injury. The ensuing lung

Copyright © 2016, the American Society of Anesthesiologists, Inc. Wolters Kluwer Health, Inc. Unauthorized reproduction of this article is prohibited.

Downloaded from http://asa2.silverchair.com/anesthesiology/article-pdf/125/5/992/270813/20161100_0-00031.pdf by guest on 09 April 2024

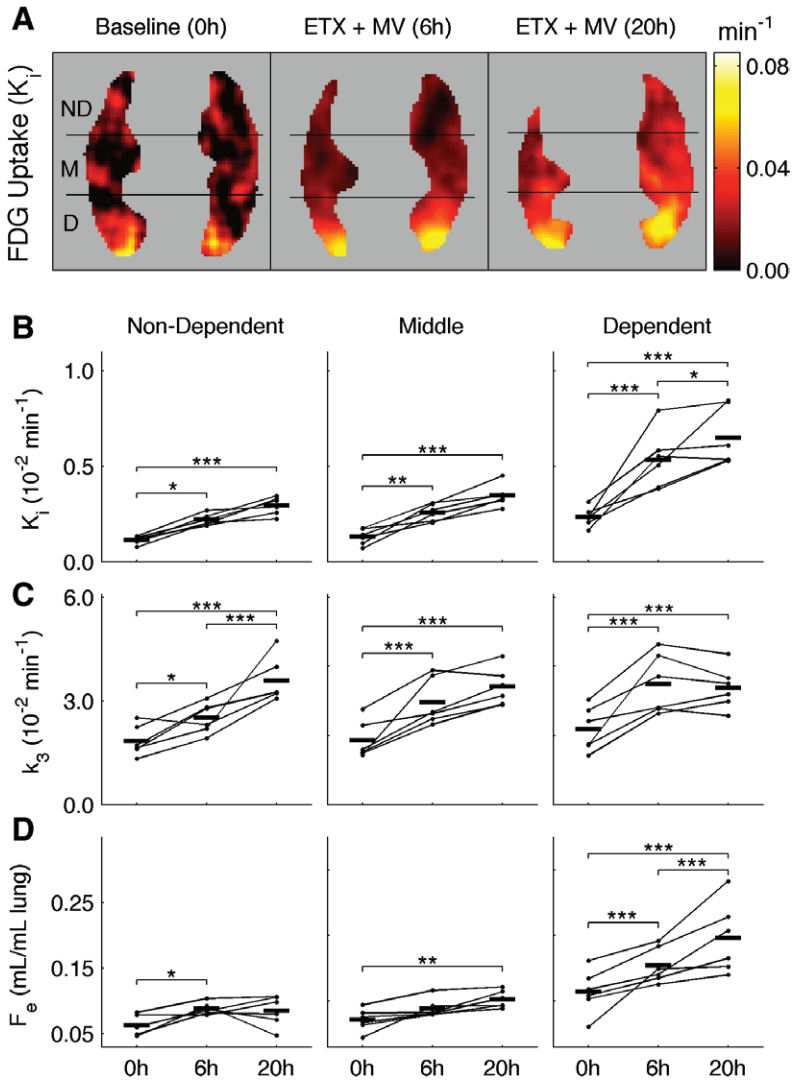

Fig. 5. Local lung inflammation, assessed from 2-deoxy-2-[(18)F]fluoro-D-glucose (^{18}F-FDG) kinetics parameters, demonstrated distinct temporal trajectories during early experimental acute respiratory distress syndrome. (*A*) The intensity and spatial heterogeneity of the ^{18}F-FDG net uptake rate (K_i) increased with time. (*A*, *B*) During the first 6 h of injury, K_i increased significantly in all lung regions and heterogeneity of K_i became more pronounced than at baseline. From 6 to 20 h, K_i continued to increase only in nondependent and middle regions. Quantification of the determinants of ^{18}F-FDG uptake ($K_i = k_3 \cdot F_e$; k_3 = phosphorylation rate; F_e = ^{18}F-FDG volume of distribution) shows the compound nature of those local metabolic changes. (*C*) k_3 increased significantly in middle and dependent regions from 0 to 6 h followed by a rise in nondependent regions from 6 to 20 h. These findings indicate an acute early development of inflammation in middle and dependent lung regions, with subsequent activation in nondependent regions only after 6 h. (*D*) Increases in the distribution volume of ^{18}F-FDG predominated in dependent regions, where they occurred throughout the experiment with larger magnitude, associated with lung derecruitment. *P < 0.05, **P < 0.01, and ***P < 0.001. ETX = endotoxemia; MV = mechanical ventilation.

collapse would result in increased regional lung strain in nondependent lung regions where VILI-related gene expression was observed. Such findings are also consistent with the observed expression of genes associated with sepsis in the dependent regions, with higher perfusion per lung tissue, in this endotoxemia model. Given that most of the FDG signal represents neutrophilic inflammation,[13,14,41] we presume that local gene expression in response to injurious events would have occurred at the time the PET signal becomes detectable. Considering our use of a current clinical ventilation protocol, our results suggest that established clinical protective standards for mechanical ventilation[15] do not entirely prevent deterioration of regional lung function and exacerbation of inflammation in the early stages of lung injury.

Using species-specific microarray technology, we detected differential regional expression of genes recently associated with human ARDS,[44] sepsis,[45] VILI,[35] and lipopolysaccharide-induced lung injury.[34] The differential expression of PAI-1 and amphiregulin is consistent with activation of coagulation[46,47] and growth factor[35] pathways during VILI. Gene expression in

Copyright © 2016, the American Society of Anesthesiologists, Inc. Wolters Kluwer Health, Inc. Unauthorized reproduction of this article is prohibited.

Downloaded from http://asa2.silverchair.com/anesthesiology/article-pdf/125/5/992/270813/20161100_0-00031.pdf by guest on 09 April 2024

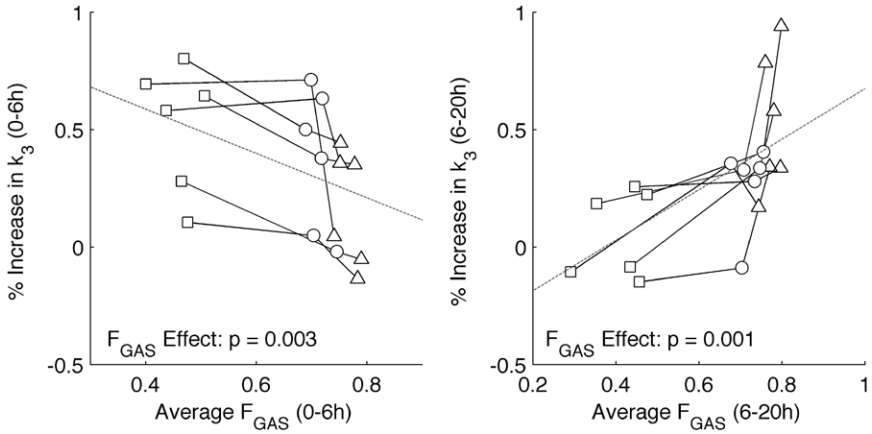

Fig. 6. The association between early and late changes in the phosphorylation rate k_3 and regional aeration is shown. During the early phase (0 to 6 h; *A*), regions of low fraction of gas (F_{GAS}; averaged over that period) showed larger increases in k_3 relative to baseline values, while during the late phase (6 to 20 h; *B*), regions of higher F_{GAS} showed larger increases in k_3. This reversal of the dependence of metabolic activity on lung aeration suggests that mechanisms of low-volume injury are associated with the initial inflammatory response followed by mechanisms of high-volume injury. The effect of F_{GAS} during each phase was analyzed using a linear mixed-effects model, including F_{GAS} as a predictor variable and random intercepts for animals. □ = dependent, ○ = middle, and Δ = nondependent regions.

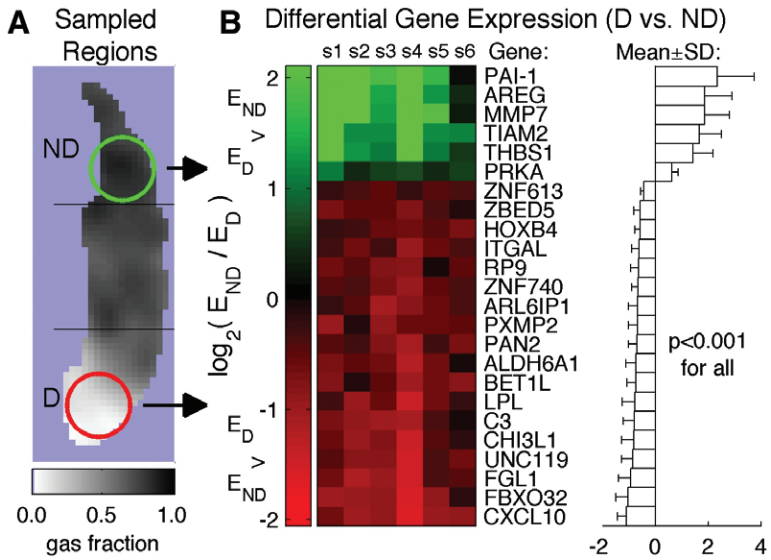

Fig. 7. Differential regional gene expression between regions of the lung with distinct function and metabolism during early experimental acute respiratory distress syndrome. (*A*) Tissue samples from nondependent (ND) and dependent (D) lung regions were analyzed using species-specific microarrays. (*B*) The heatmap shows relative expression in nondependent *versus* dependent regions (E_{ND}/E_D) on a $\log_2$ scale for genes with differential expression at $P < 0.001$ in six sheep (s1 to s6). Positive values (*green*) indicate higher nondependent expression, and negative (*red*) values indicate higher dependent expression.

dependent regions with an early increase in FDG uptake pointed to processes associated with inflammation (*e.g.*, CXCL10, C3, and CHI3L1), recruitment of inflammatory cells (*e.g.*, ITGAL), and possible changes to basic cellular machinery that might result in alterations in metabolism (*e.g.*, F-box only protein 32 [FBXO32], lipoprotein lipase [LPL], blocked early in transport 1 homolog-like [Bet1L], and aldehyde dehydrogenase 6 family member A1 [Aldh6A1]; all of which are potentially reflected by PET). In nondependent later- activated regions, there was a preponderance of genes related to the matrix/cytoskeleton (*e.g.*, matrix metalloproteinase-7 [MMP7], T-cell lymphoma invasion and metastasis 2 [TIAM2], and thrombospondin 1 [THBS1]),[1] which might reflect distention consistent with colocalized larger gas volumes. Based on previous literature, we speculate that genes related to inflammation and structural components are upregulated.[34,36,42] Instead, those related to the metabolic response may be either upregulated due to endotoxin exposure with higher perfusion in dependent regions[34] or downregulated due to stretch in nondependent regions.[42] Because our measurements express the gene expression ratio between the two studied lung regions, we are unable to determine activated *versus* suppressed genes. Since some identified genes have uncertain function and

Copyright © 2016, the American Society of Anesthesiologists, Inc. Wolters Kluwer Health, Inc. Unauthorized reproduction of this article is prohibited.

Downloaded from http://asa2.silverchair.com/anesthesiology/article-pdf/125/5/992/270813/20161100_0-00031.pdf by guest on 09 April 2024

even those with described function might have additional as yet undetermined roles, the identified genes could serve as targets to be further explored to define gene expression regulation in the early stages of ARDS. Indeed, such identified differentially regulated genes not as yet associated with lung injury may represent novel therapeutic and biomarker targets.

The gene with the most significant differential expression was that of CXCL10, a chemokine, which binds to the receptor CXCR3 to stimulate monocytes, natural killer, and T-cell migration and modulate adhesion molecule expression. Whereas recent studies suggest that CXCL10 directly contributes to neutrophil-mediated pulmonary inflammation in viral and nonviral lung injury[44,48] and human mortality after septic shock,[45] this cytokine has not yet been associated with VILI. Our preliminary murine studies (R. M. Baron, M.D., Department of Medicine - Pulmonary and Critical Care, Brigham and Women's Hospital, Harvard Medical School, Boston, Massachusetts; RT-PCR measurements of lung tissue expression of CXCL10 in control and VILI-exposed mice, unpublished data, 2015) implicate CXCL10 in sterile inflammation resulting purely from mechanical processes, raising the possibility that the regional data in sheep could indicate that those same mechanisms contribute to early injury in dependent lung regions. This is potentially important given the distinct pathways governing mechanotransduction and the few available effective clinical interventions, which include strategies that minimize mechanical forces within the lung. Our results combined with recent findings[30,44,48] suggest that CXCL10 may contribute to the local development of pulmonary neutrophilic inflammation in early ARDS in conditions frequently encountered in intensive care.

We also identified other potentially important molecular pathways, such as the C3 gene. C3 is indispensable in the complement cascade and was recently implicated in rodent VILI, representing a possible treatment target.[49,50] Interestingly, our differentially expressed genes overlap minimally with recent findings in exaggerated mechanical ventilation in rats.[46,51] This discrepancy may relate to the experimental model, applied mechanical forces (within clinical limits in our study), study duration, exposure to endotoxin, animal species, and tissue-sampling locations.

The use of blood or whole-lung lavage samples to detect biomarkers of early ARDS could overlook localized changes in gene expression or metabolism, particularly in view of individual variability in gene expression (fig. S10, Supplemental Digital Content, http://links.lww.com/ALN/B315). Topographic genomic analysis guided by functional and metabolic PET appeared highly effective in identifying genes and pathways with differential regional expression. While CT imaging has been previously used to direct genomic analysis,[36] guidance to localized biologic processes should ideally be based on molecular imaging techniques sensitive to changes in relevant lung biology. In future studies, such approaches may greatly increase the efficiency and informational yield of gene expression studies on lung injury, potentially establishing a new paradigm for deriving mechanistic information, early biomarkers, and novel targets for drug development. The fact that our imaging methods are immediately applicable to patients[52,53] underscores their potential application for individualized patient care.

In conclusion, we show that increases in cellular metabolic activation are topographically and temporally heterogeneous in the early stages of lung injury in sheep with lung sizes and functional heterogeneities comparable to those of humans. The observed metabolic activation preceded increases in lung density, which are routinely used for the clinical diagnosis of ARDS, and was accompanied by differential expression of genes and pathways known to be involved in lung injury, as well as potentially novel pathways that could be relevant for further understanding of acute lung injury and use as drug targets.

Acknowledgments

The authors thank Steve Weise, Department of Radiology (Nuclear Medicine and Molecular Imaging), Massachusetts General Hospital, Boston, Massachusetts, for the expert technical support with positron emission tomographic imaging acquisition and reconstruction and the cyclotron staff John A. Correia, Ph.D., William M. Buceliewicz, and David F. Lee, B.S., Department of Radiology (Nuclear Medicine and Molecular Imaging), Massachusetts General Hospital, Boston, Massachusetts, for preparation of the radioisotopes. The authors also thank J. Wiener-Kronish, M.D., Department of Anesthesia, Critical Care and Pain Medicine, Massachusetts General Hospital, Boston, Massachusetts, and Bela Suki, Ph.D., Biomedical Engineering, Boston University College of Engineering, Boston, Massachusetts, for criticism on the manuscript.

Research Support

Supported by R01 grants HL086827 and HL121228 from the National Heart, Lung, and Blood Institute (Bethesda, Maryland; to Dr. Vidal Melo). Dr. Musch was funded by R01HL094639 from the National Heart, Lung, and Blood Institute.

Competing Interests

Dr. Raby is a board member for and holds equity in CureSpark, Inc. (Wilmington, Delaware). Dr. Harris provided consulting services to Merck (Boston, Massachusetts). Dr. Vidal Melo received an investigator-initiated grant from Merck. The other authors declare no competing interests.

Correspondence

Address correspondence to Dr. Vidal Melo: Department of Anesthesia, Critical Care and Pain Medicine, Massachusetts General Hospital, 55 Fruit Street, Boston, MA 02114. VidalMelo.Marcos@mgh.harvard.edu. Information on purchasing reprints may be found at www.anesthesiology.org or on the masthead page at the beginning of this issue. Anesthesiology's articles are made freely accessible to all readers, for personal use only, 6 months from the cover date of the issue.

Downloaded from http://asa2.silverchair.com/anesthesiology/article-pdf/125/5/992/270813/20161100_0-00031.pdf by guest on 09 April 2024

Copyright © 2016, the American Society of Anesthesiologists, Inc. Wolters Kluwer Health, Inc. Unauthorized reproduction of this article is prohibited.

References

1. Rubenfeld GD, Caldwell E, Peabody E, Weaver J, Martin DP, Neff M, Stern EJ, Hudson LD: Incidence and outcomes of acute lung injury. N Engl J Med 2005; 353:1685–93
2. Ranieri VM, Rubenfeld GD, Thompson BT, Ferguson ND, Caldwell E, Fan E, Camporota L, Slutsky AS; ARDS Definition Task Force: Acute respiratory distress syndrome: The Berlin definition. JAMA 2012; 307:2526–33
3. Ashbaugh DG, Bigelow DB, Petty TL, Levine BE: Acute respiratory distress in adults. Lancet 1967; 2:319–23
4. Suki B, Hubmayr R: Epithelial and endothelial damage induced by mechanical ventilation modes. Curr Opin Crit Care 2014; 20:17–24
5. Wellman TJ, Winkler T, Costa EL, Musch G, Harris RS, Zheng H, Venegas JG, Vidal Melo MF: Effect of local tidal lung strain on inflammation in normal and lipopolysaccharide-exposed sheep. Crit Care Med 2014; 42:e491–500
6. Muscedere JG, Mullen JB, Gan K, Slutsky AS: Tidal ventilation at low airway pressures can augment lung injury. Am J Respir Crit Care Med 1994; 149:1327–34
7. Mead J, Takishima T, Leith D: Stress distribution in lungs: A model of pulmonary elasticity. J Appl Physiol 1970; 28:596–608
8. Huh D, Fujioka H, Tung YC, Futai N, Paine R 3rd, Grotberg JB, Takayama S: Acoustically detectable cellular-level lung injury induced by fluid mechanical stresses in microfluidic airway systems. Proc Natl Acad Sci USA 2007; 104:18886–91
9. Greenfield LJ, Ebert PA, Benson DW: Effect of positive pressure ventilation on surface tension properties of lung extracts. Anesthesiology 1964; 25:312–6
10. Schuster DP, Anderson C, Kozlowski J, Lange N: Regional pulmonary perfusion in patients with acute pulmonary edema. J Nucl Med 2002; 43:863–70
11. Costa EL, Musch G, Winkler T, Schroeder T, Harris RS, Jones HA, Venegas JG, Vidal Melo MF: Mild endotoxemia during mechanical ventilation produces spatially heterogeneous pulmonary neutrophilic inflammation in sheep. Anesthesiology 2010; 112:658–69
12. Janz DR, Ware LB: The needle in the haystack: Searching for biomarkers in acute respiratory distress syndrome. Crit Care 2013; 17:192
13. de Prost N, Feng Y, Wellman T, Tucci MR, Costa EL, Musch G, Winkler T, Harris RS, Venegas JG, Chao W, Vidal Melo MF: 18F-FDG kinetics parameters depend on the mechanism of injury in early experimental acute respiratory distress syndrome. J Nucl Med 2014; 55:1871–7
14. Musch G, Venegas JG, Bellani G, Winkler T, Schroeder T, Petersen B, Harris RS, Melo MF: Regional gas exchange and cellular metabolic activity in ventilator-induced lung injury. Anesthesiology 2007; 106:723–35
15. The Acute Respiratory Distress Syndrome Network. Ventilation with lower tidal volumes as compared with traditional tidal volumes for acute lung injury and the acute respiratory distress syndrome. N Engl J Med 2000; 342:1301–8
16. Mandava S, Kolobow T, Vitale G, Foti G, Aprigliano M, Jones M, Müller E: Lethal systemic capillary leak syndrome associated with severe ventilator-induced lung injury: An experimental study. Crit Care Med 2003; 31:885–92
17. Kolobow T, Moretti MP, Fumagalli R, Mascheroni D, Prato P, Chen V, Joris M: Severe impairment in lung function induced by high peak airway pressure during mechanical ventilation. An experimental study. Am Rev Respir Dis 1987; 135:312–5
18. Martin TR, Matute-Bello G: Experimental models and emerging hypotheses for acute lung injury. Crit Care Clin 2011; 27:735–52
19. Musch G, Bellani G, Vidal Melo MF, Harris RS, Winkler T, Schroeder T, Venegas JG: Relation between shunt, aeration, and perfusion in experimental acute lung injury. Am J Respir Crit Care Med 2008; 177:292–300
20. O'Neill K, Venegas JG, Richter T, Harris RS, Layfield JD, Musch G, Winkler T, Melo MF: Modeling kinetics of infused 13NN-saline in acute lung injury. J Appl Physiol 2003; 95:2471–84
21. Vidal Melo MF, Layfield D, Harris RS, O'Neill K, Musch G, Richter T, Winkler T, Fischman AJ, Venegas JG: Quantification of regional ventilation-perfusion ratios with PET. J Nucl Med 2003; 44:1982–91
22. Harris RS, Willey-Courand DB, Head CA, Galletti GG, Call DM, Venegas JG: Regional VA, Q, and VA/Q during PLV: Effects of nitroprusside and inhaled nitric oxide. J Appl Physiol 2002; 92:297–312
23. Treppo S, Mijailovich SM, Venegas JG: Contributions of pulmonary perfusion and ventilation to heterogeneity in V(A)/Q measured by PET. J Appl Physiol 1997; 82:1163–76
24. Schroeder T, Vidal Melo MF, Musch G, Harris RS, Venegas JG, Winkler T: Image-derived input function for assessment of 18F-FDG uptake by the inflamed lung. J Nucl Med 2007; 48:1889–96
25. Sokoloff L, Reivich M, Kennedy C, Des Rosiers MH, Patlak CS, Pettigrew KD, Sakurada O, Shinohara M: The [14C]deoxyglucose method for the measurement of local cerebral glucose utilization: Theory, procedure, and normal values in the conscious and anesthetized albino rat. J Neurochem 1977; 28:897–916
26. Dittrich AS, Winkler T, Wellman T, de Prost N, Musch G, Harris RS, Vidal Melo MF: Modeling 18F-FDG kinetics during acute lung injury: Experimental data and estimation errors. PLoS One 2012; 7:e47588
27. Ren H, Li L, Su H, Xu L, Wei C, Zhang L, Li H, Liu W, Du L: Histological and transcriptome-wide level characteristics of fetal myofiber hyperplasia during the second half of gestation in Texel and Ujumqin sheep. BMC Genomics 2011; 12:411
28. Hsia CC, Hyde DM, Ochs M, Weibel ER; ATS/ERS Joint Task Force on Quantitative Assessment of Lung Structure: An official research policy statement of the American Thoracic Society/European Respiratory Society: Standards for quantitative assessment of lung structure. Am J Respir Crit Care Med 2010; 181:394–418
29. Pássaro CP, Silva PL, Rzezinski AF, Abrantes S, Santiago VR, Nardelli L, Santos RS, Barbosa CM, Morales MM, Zin WA, Amato MB, Capelozzi VL, Pelosi P, Rocco PR: Pulmonary lesion induced by low and high positive end-expiratory pressure levels during protective ventilation in experimental acute lung injury. Crit Care Med 2009; 37:1011–7
30. Cuenca AG, Wynn JL, Kelly-Scumpia KM, Scumpia PO, Vila L, Delano MJ, Mathews CE, Wallet SM, Reeves WH, Behrns KE, Nacionales DC, Efron PA, Kunkel SL, Moldawer LL: Critical role for CXC ligand 10/CXC receptor 3 signaling in the murine neonatal response to sepsis. Infect Immun 2011; 79:2746–54
31. Kornblit B, Hellemann D, Munthe-Fog L, Bonde J, Strøm JJ, Madsen HO, Johansen JS, Garred P: Plasma YKL-40 and CHI3L1 in systemic inflammation and sepsis-experience from two prospective cohorts. Immunobiology 2013; 218:1227–34
32. Flierl MA, Rittirsch D, Nadeau BA, Day DE, Zetoune FS, Sarma JV, Huber-Lang MS, Ward PA: Functions of the complement components C3 and C5 during sepsis. FASEB J 2008; 22:3483–90
33. Gao XP, Liu Q, Broman M, Predescu D, Frey RS, Malik AB: Inactivation of CD11b in a mouse transgenic model protects against sepsis-induced lung PMN infiltration and vascular injury. Physiol Genomics 2005; 21:230–42
34. dos Santos CC, Okutani D, Hu P, Han B, Crimi E, He X, Keshavjee S, Greenwood C, Slutsky AS, Zhang H, Liu M: Differential gene profiling in acute lung injury identifies injury-specific gene expression. Crit Care Med 2008; 36:855–65

Downloaded from http://asa2.silverchair.com/anesthesiology/article-pdf/125/5/992/270813/20161100_0-00031.pdf by guest on 09 April 2024

Copyright © 2016, the American Society of Anesthesiologists, Inc. Wolters Kluwer Health, Inc. Unauthorized reproduction of this article is prohibited.

35. Dolinay T, Kaminski N, Felgendreher M, Kim HP, Reynolds P, Watkins SC, Karp D, Uhlig S, Choi AM: Gene expression profiling of target genes in ventilator-induced lung injury. Physiol Genomics 2006; 26:68–75
36. Simon BA, Easley RB, Grigoryev DN, Ma SF, Ye SQ, Lavoie T, Tuder RM, Garcia JG: Microarray analysis of regional cellular responses to local mechanical stress in acute lung injury. Am J Physiol Lung Cell Mol Physiol 2006; 291:L851–61
37. Huang da W, Sherman BT, Lempicki RA: Systematic and integrative analysis of large gene lists using DAVID bioinformatics resources. Nat Protoc 2009; 4:44–57
38. Bellani G, Messa C, Guerra L, Spagnolli E, Foti G, Patroniti N, Fumagalli R, Musch G, Fazio F, Pesenti A: Lungs of patients with acute respiratory distress syndrome show diffuse inflammation in normally aerated regions: A [18F]-fluoro-2-deoxy-D-glucose PET/CT study. Crit Care Med 2009; 37:2216–22
39. Borges JB, Costa EL, Bergquist M, Lucchetta L, Widström C, Maripuu E, Suarez-Sipmann F, Larsson A, Amato MB, Hedenstierna G: Lung inflammation persists after 27 hours of protective Acute Respiratory Distress Syndrome Network Strategy and is concentrated in the nondependent lung. Crit Care Med 2015; 43:e123–32
40. Okazumi S, Isono K, Enomoto K, Kikuchi T, Ozaki M, Yamamoto H, Hayashi H, Asano T, Ryu M: Evaluation of liver tumors using fluorine-18-fluorodeoxyglucose PET: Characterization of tumor and assessment of effect of treatment. J Nucl Med 1992; 33:333–9
41. Saha D, Takahashi K, de Prost N, Winkler T, Pinilla-Vera M, Baron RM, Vidal Melo MF: Micro-autoradiographic assessment of cell types contributing to 2-deoxy-2-[(18)F]fluoro-D-glucose uptake during ventilator-induced and endotoxemic lung injury. Mol Imaging Biol 2013; 15:19–27
42. Copland IB, Kavanagh BP, Engelberts D, McKerlie C, Belik J, Post M: Early changes in lung gene expression due to high tidal volume. Am J Respir Crit Care Med 2003; 168:1051–9
43. Schmidt EP, Yang Y, Janssen WJ, Gandjeva A, Perez MJ, Barthel L, Zemans RL, Bowman JC, Koyanagi DE, Yunt ZX, Smith LP, Cheng SS, Overdier KH, Thompson KR, Geraci MW, Douglas IS, Pearse DB, Tuder RM: The pulmonary endothelial glycocalyx regulates neutrophil adhesion and lung injury during experimental sepsis. Nat Med 2012; 18:1217–23
44. Ichikawa A, Kuba K, Morita M, Chida S, Tezuka H, Hara H, Sasaki T, Ohteki T, Ranieri VM, dos Santos CC, Kawaoka Y, Akira S, Luster AD, Lu B, Penninger JM, Uhlig S, Slutsky AS, Imai Y: CXCL10-CXCR3 enhances the development of neutrophil-mediated fulminant lung injury of viral and nonviral origin. Am J Respir Crit Care Med 2013; 187:65–77
45. Thair SA, Walley KR, Nakada TA, McConechy MK, Boyd JH, Wellman H, Russell JA: A single nucleotide polymorphism in NF-κB inducing kinase is associated with mortality in septic shock. J Immunol 2011; 186:2321–8
46. Nonas SA, Moreno-Vinasco L, Vinasco LM, Ma SF, Jacobson JR, Desai AA, Dudek SM, Flores C, Hassoun PM, Sam L, Ye SQ, Moitra J, Barnard J, Grigoryev DN, Lussier YA, Garcia JG: Use of consomic rats for genomic insights into ventilator-associated lung injury. Am J Physiol Lung Cell Mol Physiol 2007; 293:L292–302
47. Chen CM, Chou HC, Wang LF, Lang YD: Captopril decreases plasminogen activator inhibitor-1 in rats with ventilator-induced lung injury. Crit Care Med 2008; 36:1880–5
48. Wang W, Yang P, Zhong Y, Zhao Z, Xing L, Zhao Y, Zou Z, Zhang Y, Li C, Li T, Wang C, Wang Z, Yu X, Cao B, Gao X, Penninger JM, Wang X, Jiang C: Monoclonal antibody against CXCL-10/IP-10 ameliorates influenza A (H1N1) virus induced acute lung injury. Cell Res 2013; 23:577–80
49. Takahashi K, Saha D, Shattino I, Pavlov VI, Stahl GL, Finnegan P, Melo MF: Complement 3 is involved with ventilator-induced lung injury. Int Immunopharmacol 2011; 11:2138–43
50. Ngiam N, Peltekova V, Engelberts D, Otulakowski G, Post M, Kavanagh BP: Early growth response-1 worsens ventilator-induced lung injury by up-regulating prostanoid synthesis. Am J Respir Crit Care Med 2010; 181:947–56
51. Park MS, He Q, Edwards MG, Sergew A, Riches DW, Albert RK, Douglas IS: Mitogen-activated protein kinase phosphatase-1 modulates regional effects of injurious mechanical ventilation in rodent lungs. Am J Respir Crit Care Med 2012; 186:72–81
52. Harris RS, Venegas JG, Wongviriyawong C, Winkler T, Kone M, Musch G, Vidal Melo MF, de Prost N, Hamilos DL, Afshar R, Cho J, Luster AD, Medoff BD: ^{18}F-FDG uptake rate is a biomarker of eosinophilic inflammation and airway response in asthma. J Nucl Med 2011; 52:1713–20
53. Vidal Melo MF, Winkler T, Harris RS, Musch G, Greene RE, Venegas JG: Spatial heterogeneity of lung perfusion assessed with (13)N PET as a vascular biomarker in chronic obstructive pulmonary disease. J Nucl Med 2010; 51:57–65

Downloaded from http://asa2.silverchair.com/anesthesiology/article-pdf/125/5/992/270813/20161100_0-00031.pdf by guest on 09 April 2024

Copyright © 2016, the American Society of Anesthesiologists, Inc. Wolters Kluwer Health, Inc. Unauthorized reproduction of this article is prohibited.